Review

Algorithms for the Automated Analysis of Age-Related Macular Degeneration Biomarkers on Optical Coherence Tomography: A Systematic Review

Maximilian W.M. Wintergerst[1], Thomas Schultz[2], Johannes Birtel[1], Alexander K. Schuster[3], Norbert Pfeiffer[3], Steffen Schmitz-Valckenberg[1], Frank G. Holz[1], and Robert P. Finger[1]

[1] Department of Ophthalmology, University of Bonn, Bonn, Germany
[2] Department of Computer Science, University of Bonn, Bonn, Germany
[3] Department of Ophthalmology, University Medical Center Mainz, Mainz, Germany

Purpose: To assess the quality of optical coherence tomography (OCT) grading algorithms for retinal biomarkers of age-related macular degeneration (AMD).

Methods: Following a systematic review of the literature data on detection and quantification of AMD retinal biomarkers by available algorithms were extracted and descriptively synthesized. Algorithm quality was assessed using a modified version of the Quality Assessment of Diagnostic Accuracy Studies 2 checklist with a focus on accuracy against established reference standards and risk of bias.

Results: Thirty five studies reporting computer-aided diagnosis (CAD) tools for qualitative analysis or algorithms for quantitative analysis were identified. Compared with manual assessment in reference standards correlation coefficients ranged from 0.54 to 0.97 for drusen, 0.80 to 0.98 for geographic atrophy (GA), and 0.30 to 0.98 for intra- or subretinal fluid and pigment epithelial detachment (PED) detection by automated algorithms. CAD tools achieved area under the curve (AUC) values of 0.94 to 0.99, sensitivity of 0.90 to 1.00, and specificity of 0.89 to 0.92.

Conclusions: Automated analysis of AMD biomarkers on OCT is promising. However, most of the algorithm validation was performed in preselected patients, exhibiting the targeted biomarker only. In addition, type and quality of reported algorithm validation varied substantially.
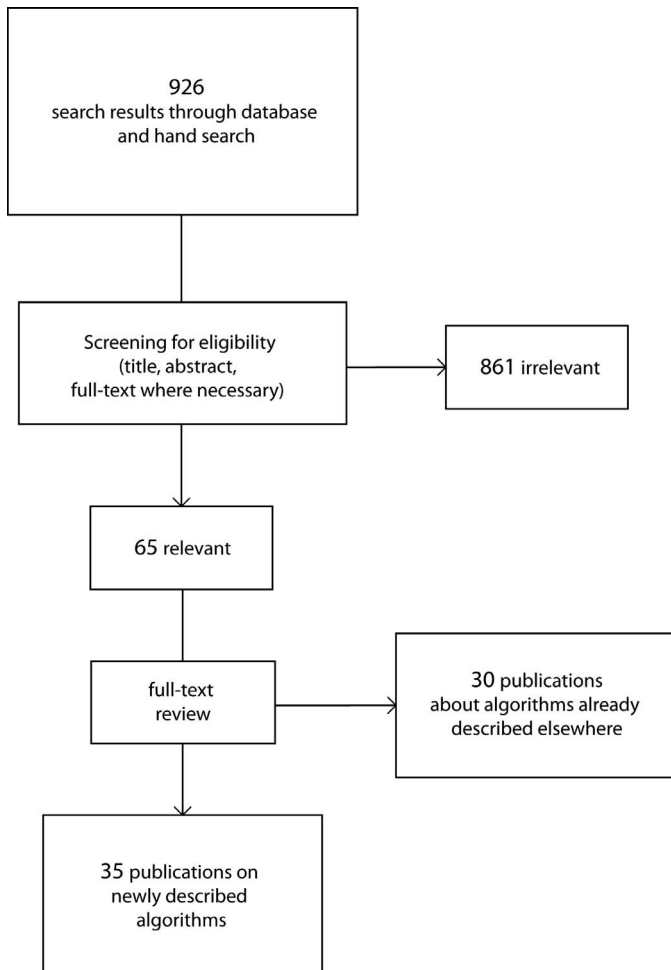
Translational Relevance: The development of algorithms for combined, simultaneous analysis of multiple AMD biomarkers including AMD staging and the agreement on standardized validation procedures would be of considerable translational value for the clinician and the clinical researcher.

Introduction

To increase our understanding of risk factors for the onset and progression of age-related macular degeneration (AMD), the leading cause of irreversible severe vision loss among Caucasians in all developed countries, we need large, prospective epidemiological studies.[1] In order to accurately stage AMD and assess progression, we increasingly rely on multimodal retinal imaging in a clinical context. This has not yet been translated into epidemiological studies, as the manual grading of the increasing data volumes generated in multimodal imaging is unfeasible. Thus, semi- or fully automated algorithms are necessary to grade image data generated in epidemiological studies.

Optical coherence tomography (OCT) is an integral part of multimodal imaging and of increasing importance in standard clinical care. The image data volume generated by OCT is particularly high (up to

```
926
search results through database
and hand search

Screening for eligibility
(title, abstract,
full-text where necessary)          →    861 irrelevant

65 relevant

full-text
review                               →    30 publications
                                          about algorithms already
                                          described elsewhere

35 publications on
newly described
algorithms
```

Figure 1. Flowchart depicting the literature search on algorithms for analysis of AMD biomarkers on OCT.

hundreds of B-Scans per examination), its manual analysis can consume a tremendous amount of time and, to date, we lack established and validated means of semi- or fully automated grading for AMD biomarkers on OCT. The first, very general approach in automated OCT analysis was automated retinal layer segmentation with subsequent thickness calculations, which can be helpful in a variety of retinal diseases as an unspecific diagnostic marker.[2] However, automated segmentation implemented in proprietary OCT software is of varying quality and frequently encounters segmentation errors in the presence of retinal pathology.[3–5] Recently, substantial efforts have been made to develop automated image analysis for detection of AMD-specific biomarkers, like drusen, geographic atrophy (GA), and sub- and intraretinal fluid, enabling a more detailed quantification of these biomarkers.

Thus, in this article we present an overview of the currently available algorithms for semi- and fully automated OCT image analysis of retinal AMD biomarkers.

Methods

Eligibility Criteria for Considering Studies for This Review

Search Methods for Identifying Studies

Our search strategy, selection of publications, and reporting of results were conducted in accordance with the Cochrane recommendations for systematic reviews. Literature was searched in MEDLINE, MEDLINE In-Process, Science Citation Index Expanded, Conference Proceedings Citation Index - Science, Book Citation Index - Science, Emerging Sources Citation Index, Korean Citation Index, and Scientific Electronic Library Online Citation Index for published studies up to March 2016. Detailed information about the search terms and formulas can be found in Supplementary Table S1. The initial search yielded 926 articles. After screening of all abstracts for eligibility, 65 references were included in the full-text review (Fig. 1). Study authors were contacted to provide additional data if required. Reference lists of manuscripts reviewed in full were hand searched for additional relevant articles. All included studies reported having obtained ethics approval.

Study Selection

Articles reporting algorithms quantifying or qualitatively analyzing retinal biomarkers of AMD on OCT images were included. Studies using OCT angiography or polarization-sensitive OCT were excluded, as were nonhuman studies. A huge body of literature is available on the general topic of automated OCT image analysis and much of it may, with some modifications, be applicable to AMD. However, in order to limit the scope of our already quite extensive survey, we decided to exclude works that did not report qualitative or quantitative AMD biomarker analysis. For example, studies improving visualization only or reporting retinal layer segmentation or retinal thickness measurements only were deemed irrelevant for this review. In case of any uncertainty a senior investigator (RPF) was consulted. Conference abstracts were excluded in case they were later published as a journal article, which was included in the review.

Data Collection and Risk of Bias Assessment

Data on OCT devices and image acquisition protocols, number of included eyes, used reference standards, algorithm functionality, validity, reliability, limitations, relations to other algorithms, key conclusions of the authors, and other relevant information were extracted. Two independent assessors (MWMW and JB) used a modified version of the Quality Assessment of Diagnostic Accuracy Studies 2 (QUADAS-2) checklist (see Supplementary Table S2 for details), which was adapted to the requirements for assessment of automated OCT analysis by including the following: algorithm training/development and testing in separate patient collectives, objective comparison to reference standard with index test, manual double grading for the reference standard, and blinding of graders and intragrader repeatability. Risk of bias was assessed regarding patient selection, conduct, and interpretation of index and reference tests and flow and timing. Agreement on study quality was high between both assessors with a kappa score of 0.85. Any ambiguities were adjudicated by a senior investigator (RPF). Risk of bias was defined as high if it was increased in any of the aforementioned fields. A summarizing statement regarding increased risk of bias is included in Tables 1 through 5. Detailed assessments of risk of bias are provided in Supplementary Table S2.

Data Synthesis and Analysis

Algorithms were categorized based on qualitative or quantitative analysis, and the latter were further categorized dependent on the analyzed biomarkers. Quality of the algorithms was assessed by comparison of their reported accuracy with the reference standard employed in each respective study as well as by assessing the appropriateness of chosen reference standards and validation samples.

Results

We identified a total of 35 algorithms for automated or semiautomated analysis of retinal AMD biomarkers on OCT (Fig. 1). These include 27 for quantitative and eight for qualitative assessment. Algorithms for the quantitative analysis include the following biomarkers: drusen, GA, pigment epithelial detachment (PED), and intra-/subretinal fluid (Fig. 2). Algorithms for qualitative analysis will be referred to as computer-aided diagnosis (CAD) tools. The algorithm characteristics are summarized
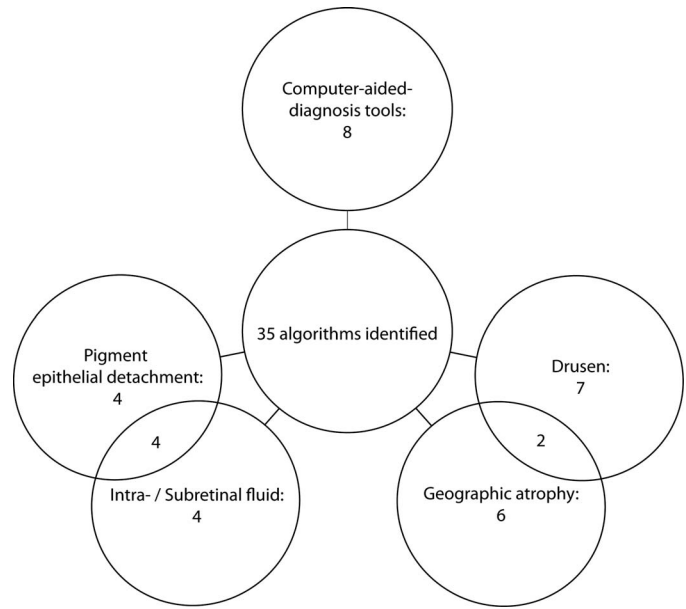
Figure 2. Overview of the entity of included algorithms.

in Tables 1 through 5. Quantitative algorithms will be presented by detected biomarker. For each category, one exemplary algorithm is presented in brief and interesting aspects of additional algorithms are highlighted.

In brief, algorithmic image analysis is based on intensity values, intensity gradients, and pixel position within the image, which was used to generate a segmentation of retinal layers or pathological structures. Based on the two-dimensional analysis, a three-dimensional interpolation can be generated for further analysis. En face images can be generated by axial projection, referred to as summed voxel projection (SVP). This can also be calculated for only a part of the axial intensity, resulting in a partial SVP (e.g., only for a specific part of the image, such as a segmented layer on OCT). The different image processing approaches used by the reviewed algorithms are listed in Supplementary Table S3.

Drusen

Seven algorithms were published on drusen detection, mainly focusing on area covered by drusen and total drusen volume, but also on drusen number and maximum diameter (see Table 1). Where available, their coefficient of correlation (CC) ranged from 0.54 to 0.97 when validated against manual grading on OCT or color fundus photography (CFP). All except one algorithm[6] relied on calculation of the difference between the actual retinal pigment epithelium (RPE)

translational vision science & technology

Table 1. Algorithms for Drusen Quantification

Reference	Output	Algorithm Characteristics	Performance (Reference Standard)	Risk of Bias	Related Studies and Clinical Applications
Farsiu et al.[7]	Area, volume, number (semiautomated)	Threshold-, shortest path finding–[13] and active contours–based RPE segmentation + ideal interpolated RPE layer + manual correction	No validation	Unclear	Region of interest can be individually defined in an en face OCT image; algorithm implemented in DOCTRAP **Toth et al.[14]:** Conference abstract on this algorithm; also individual drusen characteristics like shape and internal reflectivity were mathematically determined
Jain et al.[6]	Area (semiautomated)	Active contours–based RPE segmentation + irregularities within RPE contour + manual correction	ICC: 0.94 (CFP)	Unclear	Algorithm implemented in DOCTRAP
Gregori et al.[15]	Area, volume (3- and 5-mm perifoveal circles and full scan analysis) (automated)	Proprietary RPE segmentation + ideal interpolated RPE layer	**Coefficient of variation:** drusen area: 7.5%–9.2% drusen volume: 8.0%–11.2% **Nittala et al.[16]:** ICC drusen volume: 0.94 and drusen area: 0.64 (OCT) (risk of bias: low) **Yehoshua et al.[17]:** ICC drusen area: 0.54–0.60 (CFP) (risk of bias: unclear) **Gregori et al.[18]:** ICC drusen area: 0.70–0.81 (CFP) (risk of bias: unclear)	Unclear	Algorithm was implemented in Cirrus software **Yehoshua et al.[19]:** OCT follow-up of drusen over 24 months **Diniz et al.[12]:** extension of this algorithm for drusen number calculation **Gregori et al.[18]:** OCT follow-up of drusen over 6 months **Nathoo et al.[20]:** algorithm used for prediction of GA development based on drusen load **Diniz et al.[21]:** used this algorithm for cross-sectional study to analyze association of drusen area and volume with demographic features

translational vision science & technology

Table 1. Continued

Reference	Output	Algorithm Characteristics	Performance (Reference Standard)	Risk of Bias	Related Studies and Clinical Applications
Iwama et al.[11]	Area, maximal diameter in en face (automated)	Threshold-based RPE segmentation + Bruch's membrane calculation + edge detection in en face OCT image	**Agreement within AREDS grading system:** maximum drusen size: 94.4%, drusen area: 77.8% (CFP) **Segmentation failures:** in 3.13% of all images (criteria of Ishikawa et al.[22] were used)	High (index test)	
Chen et al.[9]	Area, volume (automated)	Threshold-based RPE segmentation + ideal interpolated RPE layer	CC drusen area: 0.94–0.97 OR (SD): 76.3 (+-11.3) % - 67.2 (+-9.14)% (OCT)	High (flow and timing)	OCT follow-up of drusen for 1 patient for nearly 3 years in this study; **de Sisternes et al.[10]:** extension of this algorithm for a total of 11 drusen features, OCT follow-up of drusen over 5 years
de Sisternes et al.[10]	11 drusen features (automated)	Features derived from segmentation using algorithm by Chen et al.[9]: drusen shape, geometry and reflectivity, drusen number, mean area, and volume per druse, maximum drusen height, total drusen area, density of affected area, and slope and texture properties of drusen.	Focus is on predicting disease progression: AUC: 0.74 (sensitivity/specificity: 81.0%, 51.2%) Accuracy of derived features as such is not validated	Unclear	Algorithm is based on the drusen detection algorithm by **Chen et al.[9]**; An algorithm for likelihood of progression from early/intermediate AMD to exudative AMD calculation was developed based on an OCT follow-up of drusen over 5 years

Table 1. Continued

Reference	Output	Algorithm Characteristics	Performance (Reference Standard)	Risk of Bias	Related Studies and Clinical Applications
Diniz et al.[12]	Number (automated)	Identification and counting of drusen clusters in Cirrus-derived RPE elevation map	**Mean drusen number (SD):** 13.2 (±3.19) in automated OCT vs. 53.7 (±13.2) in manual CFP analysis vs. 100 (±16.2) in manual IR analysis **Bland-Altman plots:** increasing underestimation of Drusen number with increasing drusen amount	Unclear	Extension for algorithm from **Gregori G. et al.**[15] for drusen number and individual drusen size calculation

AUC, area under the curve; CFP, color fundus photography; DOCTRAP, Duke OCT retinal analysis program; ICC, intraclass correlation; IR, infrared; OR, overlap ratio; SD, standard deviation.

segmentation and a calculated ideal RPE or Bruch's membrane. Two algorithms[6,7] used active contours for RPE segmentation in which an object is delineated by an energy-minimizing contour guided by the surrounding image (e.g., based on intensity gradients and internal forces dependent on the contour itself such as continuity and smoothness).[8] In the algorithm by Chen et al.,[9] the RPE was detected using an intensity threshold and interpolated to achieve a smooth line. First, an ideal RPE free of any deformations and then the difference between the ideal and real RPE layer were calculated for drusen identification. Finally, using an en face projection, possible false-positive drusen were removed if they are only present in one B-scan or based on their intensity or shape information. De Sisternes et al.[10] published an approach in which 11 drusen features, including information about drusen geometry, reflectivity, texture, number, area, and volume were used for the calculation of likelihood of progression from early and intermediate to exudative AMD. Piecewise linear regression with Lasso regularization was used and prediction of progression was estimated. A frequent limitation of algorithms for drusen detection was underestimation of overall drusen burden.[9,11,12] The authors attributed this to a "blind angle" of the algorithms for very small drusen with only minimum RPE elevation because of necessary preprocessing steps for noise reduction and absolute thresholds for RPE deviations detected as drusen.

Geographic Atrophy

Six algorithms on GA detection and area calculation were published (Table 2). Where available, their CC and overlap ratio (OR) ranged from 0.80 to 0.98 and 0.59 to 0.82, respectively, when validated against manual grading in partial OCT SVP, fundus-autofluorescence (FAF), and red-free photography (RFP). The common approach for GA detection on OCT was a partial SVP of the choroid based on the increase in reflectance intensity underneath Bruch's membrane in the area of GA. Chen et al.[23] published an exemplary algorithm using this approach. Their algorithm first segmented the RPE with an adopted version of the RPE-detection method used for their drusen detection algorithm.[9] Then, a partial SVP beneath the RPE was generated and the average axial intensity within this slab was used to generate an en face image. In the en face projection, an active contour model identified GA. In order to speed up the algorithm, a global binarization method was used to narrow down the image regions analyzed for GA. In those cases where

translational vision science & technology

Table 2. Algorithms for GA and GA + Drusen Quantification

	Reference	Output	Algorithm Characteristics	Performance (Reference Standard)	Risk of Bias	Related Studies and Clinical Applications
GA	Tsechpenakis et al.[26]	Area (semi-automated)	Active contours–based GA segmentation in partial and full SVP	OR: 98.6%–99.8% (OCT en face)	Unclear	
	Yehoshua et al.[24]	Area (automated)	Proprietary segmentation based on partial SVP	ICC: 0.80 (partial SVP) Mean area (SD): manual grading in en face OCT: 6.43 (±4.78) mm², manual grading in partial SVP: 6.41 (±4.88) mm² and automated measurement in partial SVP: 5.27 (±3.68) mm² Bland-Altman plot: larger differences with increasing lesion size. Chen et al.[23].: CC: 0.81 (FAF); OR: 59.3% (FAF)	Unclear	Algorithm was implemented in Cirrus software; Chen et al.[23]: comparison with their own algorithm Nathoo et al.[20].: algorithm used for prediction of GA development based on drusen load Diniz et al.[21].: used algorithm for cross-sectional study to analyze association of RPE atrophy area with demographic features
	Hu et al.[27]	Area (semi-automated)	Optimal surface detection–[28] and level sets–[29,30] based GA segmentation in partial SVP	Mean Dice similarity coefficient (SD): 0.87 (±0.09) Area correlation: 0.93 (partial SVP)	High (reference standard)	
	Chen et al.[23]	Area (semi-automated)	Active contours–based GA segmentation in partial SVP	CC: 0.97 (partial SVP), 0.96 (FAF) and 0.82 (Cirrus software[24]) OR: 65.9% (FAF) and 72.6% (partial SVP)	High (reference standard)	Niu et al.: (Niu S, et al. IOVS 2015;56: ARVO E-abstract 2839 advancement of this algorithm for automated detection of candidate regions of future GA development

Table 2. Continued

	Reference	Output	Algorithm Characteristics	Performance (Reference Standard)	Risk of Bias	Related Studies and Clinical Applications
	Tadarati et al.* (Tadarati M, et al.: IOVS 2015;56: ARVO E-abstract 2855)	Area (automated)	Conference abstract; details not given	CC: 0.88/0.94 (right/left eye)(CFP), 0.85/0.84 (RFP) and 0.83/0.90 (FAF)	-	
	Niu et al.[31]	Area (automated)	Level sets[29,30]-based GA segmentation in partial SVP	CC: 0.98 (OCT) and 0.94 (FAF); OR: 81.9% (OCT) and 70% (FAF)	High (reference standard)	Same two datasets for validation as in **Chen et al.**[23] were used; Algorithm accuracy compared to the algorithm of **Chen et al.**[23]
GA + drusen	Chiu et al.[25]	RPEDC volume (automated)	RPEDC segmentation based on shortest path in derived graph[13,32] + detection of drusen and atrophy via abnormal thickening and thinning	**Mean error in RPEDC thickness (SD):** 3.2 (+-2.6); **Reliability:** mean volume difference (SD) = 1.6 (±1.57)% (OCT)	unclear	Algorithm partially based on **Chiu et al.**[32]; **Farsiu et al.**[33]: CAD tool partially based on this algorithm **Folgar et al.**[34]: used this algorithm with manual correction
	Folgar et al.[34]	RPEDC volume (semi-automated)	RPEDC segmentation based on shortest path in derived graph[13,32] + manual correction + detection of drusen and atrophy via abnormal thickening and thinning	No validation	Low	DOCTRAP was used for segmentation; Algorithm from **Chiu et al.**[25] was used with manual correction; Prediction of AMD progression based on RPEDC thinning / thickening

* This reference included not enough information for risk of bias assessment. CC, coefficient of correlation; CFP, color fundus photography; DOCTRAP, Duke OCT retinal analysis program; FAF, fundus autofluorescence; GA, geographic atrophy; ICC, intraclass correlation; IR, infrared; OR, overlap ratio; RFP, red-free-photography; RPEDC, RPE-drusen-complex; SD, standard deviation; SVP, summer voxel projection.

the binarization results were far away from the real GA boundaries, a region around the GA was specified manually for further GA analysis. The algorithm was also compared with the algorithm described by Yehoshua et al.,[24] currently implemented in the Cirrus Software (Carl Zeiss Meditec, Jena, Germany). A limitation of the algorithm by Chen et al.[23] was a generally underestimated GA area.

Geographic Atrophy and Drusen

One algorithm combined GA and drusen detection and was published in a fully automated and a semiautomated version (Table 2). Chiu et al.[25] used abnormal thinning and thickening of a multiple-layer complex called RPE-drusen complex (RPEDC), defined by the inner aspect of the RPE plus drusen material and the outer aspect of Bruch's membrane, in order to identify GA and drusen, respectively. Subretinal drusenoid deposits were also included in the RPEDC. After image downsampling, binarization was used to separate the hyperreflective inner layers (retinal nerve fiber layer and the two plexiform layers) from the outer hyperreflective RPEDC. Subsequently, the internal limiting membrane, the inner border of the RPEDC and Bruch's membrane were segmented by iteratively finding shortest paths in a derived graph. In this approach, each pixel corresponds to a node, edge weights were based on intensity gradients, and shortest paths were found between the left and right image boundaries. The algorithm was less accurate on OCT scans containing both GA and drusen versus solely drusen. Beside the validation against manual segmentation on OCT, no additional statistical analysis was reported.

Pigment Epithelial Detachment

Out of four algorithms quantifying PED volume (Table 3), two[35,36] were based on the same principle of ideal to actual RPE comparison presented above, and two[37,38] used the graph-based surface segmentation approach by Li et al.[39] for fluid detection within PEDs. The first two calculated PED area as well. Three of the algorithms were validated against manual segmentation on OCT; however, different statistical methods were used. One of these was the drusen quantification algorithm developed by Gregori et al.[15] (see Table 1), which was licensed to Carl Zeiss and used for PED quantification.[38] Segmentation with this algorithm performed less well in cases with GA.[36]

Intra-/Subretinal Fluid and Pigment Epithelial Detachment

Eight algorithms on fluid-associated alterations were found, four for intra- and subretinal fluid detection only, and four that also include PEDs (see Table 4). All were validated against manual segmentation on OCT. However, the variety of statistical methods used makes a direct comparison difficult. The four algorithms detecting intra- and subretinal fluid only were based on a variety of image analysis methods such as gray level– or gradient-based segmentation, active contours, and convolutional neural networks. The latter is a state of the art machine learning technique inspired by biological neural networks within the visual cortex. The algorithms detecting intra- and subretinal fluid as well as PEDs were all graph-based and used classifiers for fluid detection, except one.[40] In brief, classifiers assign an object to a class, for example, based on the class of the k most similar objects (k nearest-neighbor classifier) or a "forest" of randomly generated decision-trees during a learning process (random forest classifier). The algorithm by Zheng et al.[41] used intensity gradient-based edge maps for segmentation of fluid-filled regions. The true positive delineated regions were then manually selected. In validation against manual OCT segmentation the dice coefficient was used, which is a commonly used measure for comparison of similarity in image analysis.

Some of the presented algorithms were implemented in the Cirrus software and are commercially available. This is the case for the algorithm developed by Gregori et al.,[15,36] which was used for drusen and PED[36] quantification and for the algorithm on GA quantification described by Yehoshua et al.[24] The implemented algorithms for drusen and GA detection got Food and Drug Administration approval as a part of the Cirrus HD-OCT 6.0 software.

Computer-Aided Diagnosis Tools

For algorithms with qualitative analysis a classification process is needed, for which machine learning algorithms are often used. In order to build a model for the classification process, the algorithm analyzes a training dataset, in which the diagnosis of all subjects is known. Then, a testing dataset is used to evaluate the model's performance. A frequently used method in machine learning are support-vector machines (SVMs), in which an optimal separating

translational vision science & technology

Table 3. Algorithms for PED Quantification

Reference	Output	Algorithm Characteristics	Performance (Reference Standard)	Risk of Bias	Related Studies and Clinical Applications
Ahlers et al.[35]	Area, volume (automated)	Threshold- and gradient-based RPE segmentation + ideal interpolated RPE calculation	**Segmentation quality subjectively assessed** (on a scale from 1 = limited quality to 5 = perfect, no errors): interpolation of ideal RPE 3.5–3.65, RPE segmentation 4.15–4.3	High (reference standard)	OCT follow up over 3 months after anti-VEGF injection in 2 patients
Penha et al.[36]	Area, volume (automated)	RPE segmentation + ideal interpolated RPE layer	**Reliability:** ICC 0.997–1.000 Ho et al.[42]: **ICC** PED volume: 0.30–0.34 (OCT); PED volume was significantly greater in manual measurement; **Reliability** for PED volume measurement: ICC 0.95–0.98 (risk of bias: unclear)	Unclear	Drusen quantification algorithm from **Gregori et al.**[15] used for PED quantification; **Penha et al.**[43]: retrospective PED volume analysis with this algorithm for prediction of anti-VEGF retreatment **Filho et al.**[44]: case report using this algorithm showing increased PED volume prior to hemorrhage
Shi et al.[38]	Volume (automated)	Multiresolution graph search of 11 surfaces defining 10 retinal layers[45]	**TPV, FPV and PPV:** for eyes with PED 87.1%, 0.37% and 81.2%, respectively; FPV in healthy eyes: 0% (OCT)	High (reference standard)	Results on the same dataset compared with algorithm of **Chen et al.**[46]
Sun et al.[37]	Volume (automated)	Multiresolution graph search[45,47] for layer segmentation; PED segmentation based on local feature based classification, AdaBoost, mathematical morphology + graph cuts[37,48]	**TPV, FPV and PPV:** 90.1%, 0.22%, 92.6% **Average dice similarity coefficient:** 91.2% (reference standard unclear)	Unclear	Results on the same dataset compared with algorithm of **Shi et al.**[38]

FPV, false positive volume; ICC, intraclass correlation; PED, pigment epithelial detachment; PPV, positive predictive value; TPV, true positive volume.

Wintergerst et al.

Table 4. Algorithms for Intra- or Subretinal Fluid and PED Quantification

	Reference	Output	Algorithm Characteristics
Intra-/ subretinal fluid	Fernandez et al.[49]	Area, volume (semiautomated)	Active contours–based segmentation of fluid regions with manual initialization
	Zheng et al.[41]	Area (semiautomated)	Gradient-based edge-maps segmentation + Split Bregman method[50,51] + manual selection (not delineation) of fluid regions
	Pilch et al.[52]	Area, volume (automated)	Gray-level segmentation based on local feature based k-means cluster analysis and k-nearest neighbor classification[48,53,54]
	Schlegl et al. (Schlegel T, et al. *IOVS* 2015;56: ARVO E-abstract 5920)	Area (automated)	Convolutional neuronal networks based individual pixel classification as normal, intraretinal fluid, or subretinal fluid[55]
Intra-/ subretinal fluid & PED	Dolejší et al.[40]	Volume (semiautomated)	Retinal layer and fluid filled region segmentation based on graph search[47] with manual initialization
	Chen et al.[46]	Volume (automated)	Segmentation of fluid-filled regions with the combination of k nearest-neighbor classification based on 52 features[48] and optimal surface detection[28]
	Ding et al.[58] (conference abstract)	Detection (automated)	Segmentation of intraretinal fluid with a combination of optimal surface detection[28,59] and a variational approach solved using the Split Bregman algorithm[50, 51]; classification as true or false positive fluid based on shape and intensity features of fluid surrounding area using a random forest classifier[60]
	Xu et al.[61]	Volume (automated)	11-layer segmentation based on graph search,[45] layer-dependent stratified sampling for fluid segmentation with a k nearest-neighbor-classifier[53] based on 52 extracted voxel features[48]

Table 4. Extended

	Reference	Performance (Reference Standard)	Risk of Bias	Related Studies and Clinical Applications
Intra-/ subretinal fluid	Fernandez et al.	**Subjective evaluation:** 95% of good or fair segmentation **Plot-based comparison** with manual segmentation on OCT	High (reference standard)	
	Zheng et al.[41]	**ICC:** 0.90–0.98 (OCT) **Dice Coefficient:** 0.72–0.79 (OCT) **Reliability:** ICC: 0.998–0.999, Dice coefficient: 0.96–0.98	Unclear	
	Pilch et al.[52]	**Bland-Altman plot:** discrepancies in area measurements were within the range of the area deviations among the experts (OCT)	Unclear	Follow-up of 1 patient with serous retinal detachment due to exudative AMD over 4 years
	Schlegl et al. (Schlegel T, et al. *IOVS* 2015;56: ARVO E-abstract 5920)	**Overlap accuracy:** healthy: 98%; intraretinal fluid: 90%; subretinal fluid: 92% (OCT)	Unclear	
Intra-/ subretinal fluid & PED	Dolejší et al.[40]	**Coefficient of determination:** 0.91 (previous semiautomated graph-cut algorithm) **Reliability:** mean volume difference 0.12 ± 0.2 mm^3	High (reference standard)	
	Chen et al.[46]	**CC:** 0.95 (OCT) **TPV, FPV, and relative volume difference ratio:** 86.5%, 1.7%, and 12.8% (OCT) **Shi et al.: TPV, FPV,** and **PPV** for PED: 84.1%, 0.44% and 81.2% (OCT)	High (reference standard)	Precursor and related algorithms: **Quellec et al.**[56] **Dolejší et al.**[40] **Niemeijer et al.**[57]
	Ding et al.[58] (conference abstract)	**Sensitivity:** 75.2% (OCT) **PPV:** 14.8% (OCT)	Unclear	
	Xu et al.[61]	**Positive and true negative rate:** 96% and 0.16% (OCT) **Coefficient of determination:** 0.997 (OCT)	Unclear	Related algorithm: **Chen et al.**[46]

CC, coefficient of correlation; FPV, false positive volume; ICC, intraclass correlation; PED, pigment epithelial detachment; PPV, positive predictive value; TPV, true positive volume.

linear boundary is generated for classification,[62] possibly after implicit nonlinear mapping to a higher-dimensional space. For mapping of the data, any OCT-derived information can be used. Eight CAD tools were identified, seven for AMD and one for PED classification. They had a variety of readouts and used different approaches (Table 5). Where available, their sensitivity and specificity ranged from 0.58 to 1.0 and 0.64 to 1.0, respectively, against the reference standard of manual classification on OCT. As an example, the algorithm by Srinivasan et al.,[63] distinguished between healthy retina, dry AMD, and diabetic macular edema (DME). A relatively small area of the B-scan, consisting of the 150 central A-scans and only the 40 pixels above and 5 pixels below the mean RPE level was cropped for analysis. For classification, histograms of oriented gradients (HOG) descriptors were used. To compute these, the image was divided into small spatial cells. For each cell, a contrast-normalized one-dimensional histogram of the directions of the spatial gradients, weighted by their magnitudes, was calculated. This process was performed four times with different properties. Three SVMs were trained to correctly classify the B-scans based on the extracted HOG features: normal versus AMD, normal versus DME, and AMD versus DME.

Discussion

Most of the algorithms identified perform well when compared with manual grading. However, the samples used for assessment of algorithm quality were small and preselected for the presence of a particular biomarker and the absence of additional pathology in most cases. In addition, availability of high-quality images suitable for algorithm development and assessment was a prerequisite for inclusion into studies. Against this background, available algorithms for the automated detection and quantification of AMD biomarkers on OCT image data are promising; however, further quality assessment as well as assessment of their performance in samples that may contain multiple pathologies, and are thus more representative of a wider utilization are warranted.

Of all AMD biomarkers, GA was detected most robustly, while the greatest variability of performance was observed in algorithms for intra-/subretinal fluid and PED detection. This might be due to a greater diversity of how the biomarker fluid can present on OCT compared with drusen and GA. While the technical approaches for the different algorithms for drusen and GA segmentation are very similar for the respective biomarker, there is a greater variability of image analysis techniques for intra-/subretinal fluid, PED, and CAD tools. This might be due to the availability of very general and easily accessible image analysis approaches for drusen and GA as well as their comparatively uniform appearance on OCT. However, although comparison of the different algorithms reported is difficult due to a lack of standardization in their quality assessment, the best overall performance seems to have been achieved by CAD tools. This is likely the case as the sole step of detecting a pathology might be less prone to errors than the combination of detecting and quantifying it.

The most impeding barrier for the comparison of identified algorithms is the inconsistency in their quality assessment. A substantial number of articles reported repeatability or a numerical comparison of measurements with the reference standard only. For most algorithms, it is unclear whether the development and evaluation of the algorithm was made in separate patient samples, which is necessary in order to prevent risk of bias and achieve reliable validation. A highly relevant question is whether an algorithm can be used in a routine, not preselected patient sample. However, in most of the reviewed studies the patient pool for testing was preselected for the respective pathology (e.g., drusen). While this is reasonable for the first stages of algorithm development, it is not representative of typical AMD patients, in whom multiple AMD biomarkers are present simultaneously. Few algorithms combining analysis of different AMD biomarkers were described so far, like the very general approaches of Chiu et al.[25] on drusen and atrophy and of Chen et al.[46] on "symptomatic exudate-associated derangements" including PEDs, intra- and subretinal fluid. Both algorithms actually measured only one feature, which comprised the respective biomarkers (RPEDC thickness in the first and fluid regions in the second).

Algorithms for quantitative analysis of retinal AMD biomarkers are not only available for OCT images but also for other imaging modalities. A significant number of algorithms for the analysis of CFP were extensively reviewed elsewhere.[74] Overall, high accuracy was achieved. These algorithms functioned with image filtering, texture-, threshold-, clustering-, and edge-based detection, and recently also included machine learning technology. In our opinion, the combination of algorithms for different

Table 5. Algorithms for Qualitative Analysis

Reference	Detected Biomarker	Algorithm Characteristics	Performance (Reference Standard)	Risk of Bias	Related Studies and Clinical Applications
Liu et al.[64]	AMD, Macular hole, and ME (semiautomated)	Local feature based support vector machine classifier[48] foveal B-scan has to be selected manually	**AUC** (training dataset/testing dataset): AMD 0.938/0.975, ME 0.939/0.941, normal 0.976/0.978 (OCT) **Sensitivity and specificity:** AMD 89.7% and 88.8%, ME 87.5% and 87.0%, healthy: 99.4% and 91.5% (OCT)	Unclear	Precursor algorithms: **Liu et al.**[65] (conference abstract) **Liu et al.**[66]
Serrano-Aguilar et al.[67]	Exudative AMD (automated)	Haar-like features—[48,68] based detection of ILM, RPE, and possible intraretinal fluids, classification with a decision tree generated using C4.5 algorithm[69]	**Sensitivity and Specificity:** 96% and 92% (OCT)	Low	
Lee et al.[70]	PED classification (automated)	Classification of each individual A-Scan in serous/fibrovascular/ drusenoid type based on mean intensity, PED classification based on predominant A-Scan classification	**Sensitivity and specificity:** 88% and 100% for serous, 76% and 64% for fibrovascular and 58% and 81% for drusenoid (OCT)	Low	
Albarrak et al.[71]	AMD (automated)	Bayesian network classifier based on local binary pattern and histogram of oriented gradient based feature extraction[48,71]	**Precision:** 91.5, **F-score:** 91.4, **accuracy:** 91.4, **sensitivity:** 92.4, **specificity:** 90.5, **AUC:** 94.4 (OCT)	Unclear	The algorithm's performance was compared with one of the precursor algorithms of **Liu et al.**[66]

translational vision science & technology

Table 5. Continued

Reference	Detected Biomarker	Algorithm Characteristics	Performance (Reference Standard)	Risk of Bias	Related Studies and Clinical Applications
Zhang et al.[72]	AMD (automated)	Custom classifier based on a kernel principle component analysis ensemble; feature extraction using local binary patterns, local phase quantization, and multiscale spatial pyramid[48,72]	**Sensitivity:** AMD: 91.8%, healthy: 92.3% (OCT)	Unclear	
Farsiu et al.[33]	Intermediate AMD (semiautomated)	Manually corrected graph theory– and dynamic programming–based segmentation[25] + generalized linear model regression–based classification	**AUC:** 0.99 (OCT)	Low	Also quantification of RPEDC; DOCTRAP was used for segmentation; Precursor algorithm: **Chiu et al.**[25]
Srinivasan et al.[63]	DME or dry AMD (automated)	Histogram of oriented gradients based support vector machine classifier	**Sensitivity:** AMD 100%, healthy 86.7% (OCT)	Unclear	
Venhuizen et al.[73]	AMD (automated)	Random forest classifier based on patch occurrence histograms	**AUC:** 0.98 (OCT)	Unclear	

AUC, area under the curve; DOCTRAP, Duke OCT retinal analysis program; ILM, internal limiting membrane; PED, pigment epithelial detachment; RPEDC, RPE-drusen-complex.

imaging modalities like CFP and OCT would be a promising approach for enhancing algorithm accuracy and allowing comprehensive disease classification.

Most of the drusen quantification algorithms for OCT calculate total drusen area and volume and do not include individual drusen parameters such as size, which are necessary for AMD classification (see Table 1). Interesting exceptions are two algorithms, in which individual drusen size was assessed.[11,12] Diniz et al.[12] differentiated small (<63 μm), intermediate (63–125 μm), and large (>125 μm) drusen, however individual drusen size was just roughly estimated under the assumption of all drusen being perfect circles (area = $\pi r^2 \rightarrow$ diameter = 2 r). Another study classified AMD on OCT according to the Age-related Eye Disease Study Grading System (AGS) using maximum drusen size and percentage of drusen area within the AGS grid.[11] These two algorithms are promising examples of how automated OCT analysis can be implemented in AMD classification of early and intermediate AMD. Classification is also available for other AMD stages: CAD tools are capable of distinguishing between healthy and early AMD[33] and healthy and exudative AMD (Schlegl T, et al. *IOVS* 2015;56: ARVO E-abstract 5920).[64,67] A classifier able to differentiate early from advanced AMD is the next step. There is already one algorithm, which partially fulfills this and can discriminate between DME and early AMD.[63] As ME can also be due to exudative AMD, this algorithm might also be capable to differentiate early from wet AMD. Other algorithms for OCT analysis for relatively unspecific retinal biomarkers like intraretinal fluid were developed for unrelated pathology, but might function similarly well in AMD (e.g., for cystoid ME in vitreoretinal disease[75] and for microcystic ME in multiple sclerosis[76]).

So far, no automated quantification of other retinal AMD biomarkers like pigmentary abnormalities, reticular pseudodrusen (RPD), changes preceding GA, and choroidal neovascularization (CNV) is available. However, pigmentary changes can be identified on OCT with a sensitivity of 66.5% and specificity of 78.7% using hyperreflectivity.[77] The algorithm for combined drusen and GA detection mentioned above[25] includes possible RDP within the analyzed RPEDC, yet differentiation from conventional drusen is not possible. One study quantified drusen-associated photoreceptor layer thinning semi-automatically.[78]

The strengths of this first review on automated OCT image analysis of AMD retinal biomarkers are its systematic approach and the standardized quality assessment of included algorithms. The main limitation of this study is the absence of a uniform quality assessment due to an inconsistent assessment of algorithm quality and performance across studies.

In conclusion, automated analysis of AMD biomarkers on OCT is promising; however, type and quality of reported algorithm validation vary substantially and most validation has been performed in preselected patients only. The development of algorithms for combined, simultaneous analysis of multiple AMD biomarkers including AMD staging and the agreement on standardized validation procedures would be of considerable translational value for the clinician and the clinical researcher.

Acknowledgments

References

1. Klein R, Klein BE, Linton KL. Prevalence of age-related maculopathy. The Beaver Dam Eye Study. *Ophthalmology*. 1992;99:933–943.
2. Hee MR, Puliafito CA, Duker JS, et al. Topography of diabetic macular edema with optical coherence tomography. *Ophthalmology*. 1998;105:360–370.
3. Schlanitz FG, Ahlers C, Sacu S, et al. Performance of drusen detection by spectral-domain optical coherence tomography. *Invest Ophthalmol Vis Sci*. 2010;51:6715–6721.
4. Schuetze C, Ahlers C, Sacu S, et al. Performance of OCT segmentation procedures to assess morphology and extension in geographic atrophy. *Acta Ophthalmol*. 2011;89:235–240.
5. Penha FM, Gregori G, Yehoshua Z, Feuer WJ, Rosenfeld PJ. Identifying the boundaries of retinal pigment epithelial detachments using two spectral-domain optical coherence tomography instruments. *Ophthalmic Surg Lasers Imaging Retina*. 2013;44:10–16.

6. Jain N, Farsiu S, Khanifar AA, et al. Quantitative comparison of drusen segmented on SD-OCT versus drusen delineated on color fundus photographs. *Invest Ophthalmol Vis Sci*. 2010;51:4875–4883.

7. Farsiu S, Chiu SJ, Izatt JA, Toth CA. Fast detection and segmentation of drusen in retinal optical coherence tomography images. *Proc. SPIE 6844*, Ophthalmic Technologies XVIII, 68440D February 11, 2008; doi:10.1117/12.768624.

8. Kass M, Witkin A, Terzopoulos D. Snakes: active contour models. *Int J Comp Vis*. 1988;1:321–331.

9. Chen Q, Leng T, Zheng L, et al. Automated drusen segmentation and quantification in SD-OCT images. *Med Image Anal*. 2013;17:1058–1072.

10. de Sisternes L, Simon N, Tibshirani R, Leng T, Rubin DL. Quantitative SD-OCT imaging biomarkers as indicators of age-related macular degeneration progression. *Invest Ophthalmol Vis Sci*. 2014;55:7093–7103.

11. Iwama D, Hangai M, Ooto S, et al. Automated assessment of drusen using three-dimensional spectral-domain optical coherence tomography. *Invest Ophthalmol Vis Sci*. 2012;53:1576–1583.

12. Diniz B, Ribeiro R, Heussen FM, Maia M, Sadda S. Drusen measurements comparison by fundus photograph manual delineation versus optical coherence tomography retinal pigment epithelial segmentation automated analysis. *Retina*. 2014;34:55–62.

13. Dijkstra EW. A note on two problems in connexion with graphs. *Numerische Mathematik*. 1959;1:269–271.

14. Toth CA, Farsiu S, Chiu SJ, Khanifar AA, Izatt JA. Automatic drusen segmentation and characterization in spectral domain optical coherence tomography (SDOCT) images of AMD eyes. *Invest Ophthalmol Vis Sci*. 2008;49:5394–5394.

15. Gregori G, Wang F, Rosenfeld PJ, et al. Spectral domain optical coherence tomography imaging of drusen in nonexudative age-related macular degeneration. *Ophthalmology*. 2011;118:1373–1379.

16. Nittala MG, Ruiz-Garcia H, Sadda SR. Accuracy and reproducibility of automated drusen segmentation in eyes with non-neovascular age-related macular degeneration. *Invest Ophthalmol Vis Sci*. 2012;53:8319–8324.

17. Yehoshua Z, Gregori G, Sadda SR, et al. Comparison of drusen area detected by spectral domain optical coherence tomography and color fundus imaging. *Invest Ophthalmol Vis Sci*. 2013;54:2429–2434.

18. Gregori G, Yehoshua Z, Garcia CAD, et al. Change in drusen area over time compared using spectral-domain optical coherence tomography and color fundus imaging. *Invest Ophthalmol Vis Sci*. 2014;55:7662–7668.

19. Yehoshua Z, Wang F, Rosenfeld PJ, Penha FM, Feuer WJ, Gregori G. Natural history of drusen morphology in age-related macular degeneration using spectral domain optical coherence tomography. *Ophthalmology*. 2011;118:2434–2441.

20. Nathoo NA, Or C, Young M, et al. Optical coherence tomography-based measurement of drusen load predicts development of advanced age-related macular degeneration. *Am J Ophthalmol*. 2014;158:757–761.

21. Diniz B, Rodger DC, Chavali VR, et al. Drusen and RPE atrophy automated quantification by optical coherence tomography in an elderly population. *Eye*. 2015;29:272–279.

22. Ishikawa H, Stein DM, Wollstein G, Beaton S, Fujimoto JG, Schuman JS. Macular segmentation with optical coherence tomography. *Invest Ophthalmol Vis Sci*. 2005;46:2012–2017.

23. Chen Q, de Sisternes L, Leng T, Zheng L, Kutzscher L, Rubin DL. Semi-automatic geographic atrophy segmentation for SD-OCT images. *Biomed Opt Express*. 2013;4:2729–2750.

24. Yehoshua Z, Garcia Filho CAA, Penha FM, et al. Comparison of geographic atrophy measurements from the oct fundus image and the sub-RPE slab image. *Ophthalmic Surg Lasers Imaging Retina*. 2013;44:127–132.

25. Chiu SJ, Izatt JA, O'Connell RV, Winter KP, Toth CA, Farsiu S. Validated automatic segmentation of AMD pathology including drusen and geographic atrophy in SD-OCT images. *Invest Ophthalmol Vis Sci*. 2012;53:53–61.

26. Tsechpenakis G, Lujan B, Martinez O, Gregori G, Rosenfeld PJ. Geometric deformable model driven by CoCRFs: application to optical coherence tomography. *Med Image Comput Comput Assist Interv*. 2008;11:883–891.

27. Hu ZH, Medioni GG, Hernandez M, Hariri A, Wu XD, Sadda SR. Segmentation of the geographic atrophy in spectral-domain optical coherence tomography and fundus autofluorescence images. *Invest Ophthalmol Vis Sci*. 2013;54:8375–8383.

28. Li K, Wu X, Chen DZ, Sonka M. Optimal surface segmentation in volumetric images-a graph-theoretic approach. *IEEE Trans Pattern Anal Mach Intell*. 2006;28:119–134.

29. Gibou F, Fedkiw R, Caflisch R, Osher S. A level set approach for the numerical simulation of dendritic growth. *J Sci Comp*. 2003;19:183–199.

30. Sethian JA. Level Set Methods and Fast Marching Methods: Evolving Interfaces in Computational Geometry, Fluid Mechanics, Computer Vision, and Materials Science. New York: Cambridge University Press; 1999.

31. Niu S, de Sisternes L, Chen Q, Leng T, Rubin DL. Automated geographic atrophy segmentation for SD-OCT images using region-based C-V model via local similarity factor. *Biomed Opt Express*. 2016;7:581–600.

32. Chiu SJ, Li XT, Nicholas P, Toth CA, Izatt JA, Farsiu S. Automatic segmentation of seven retinal layers in SDOCT images congruent with expert manual segmentation. *Opt Express*. 2010; 18:19413–19428.

33. Farsiu S, Chiu SJ, O'Connell RV, et al. Quantitative classification of eyes with and without intermediate age-related macular degeneration using optical coherence tomography. *Ophthalmology*. 2014;121:162–172.

34. Folgar FA, Yuan EL, Sevilla MB, et al. Drusen Volume and retinal pigment epithelium abnormal thinning volume predict 2-year progression of age-related macular degeneration. *Ophthalmology*. 2016;123:39–50, e31.

35. Ahlers C, Simader C, Geitzenauer W, et al. Automatic segmentation in three-dimensional analysis of fibrovascular pigmentepithelial detachment using high-definition optical coherence tomography. *Br J Ophthalmol*. 2008;92: 197–203.

36. Penha FM, Rosenfeld PJ, Gregori G, et al. Quantitative imaging of retinal pigment epithelial detachments using spectral-domain optical coherence tomography. *Am J Ophthalmol*. 2012;153: 515–523.

37. Sun Z, Chen H, Shi F, et al. An automated framework for 3D serous pigment epithelium detachment segmentation in SD-OCT images. *Sci Reports*. 2016;6:21739.

38. Shi F, Chen X, Zhao H, et al. Automated 3-D retinal layer segmentation of macular optical coherence tomography images with serous pigment epithelial detachments. *IEEE Trans Med Imaging*. 2014;34:441–452.

39. Li K, Wu X, Chen DZ, Sonka M. Optimal surface segmentation in volumetric images–a graph-theoretic approach. *IEEE Trans Pattern Anal Mach Intell*. 2006;28:119–134.

40. Dolejší M, Abràmoff MD, Sonka M, Kybic J. Semi-automated segmentation of symptomatic exudate-associated derangements (SEADs) in 3D OCT using layer segmentation. Presented at: Biosignal 2010, June 2010, Brno, Czech Republic.

41. Zheng Y, Sahni J, Campa C, Stangos AN, Raj A, Harding SP. Computerized assessment of intraretinal and subretinal fluid regions in spectral-domain optical coherence tomography images of the retina. *Am J Ophthalmol*. 2013;155: 277–286.

42. Ho J, Adhi M, Baumal C, et al. Agreement and reproducibility of retinal pigment epithelial detachment volumetric measurements through optical coherence tomography. *Retina*. 2015;35:467–472.

43. Penha FM, Gregori G, Filho C, Yehoshua Z, Feuer WJ, Rosenfeld PJ. Quantitative changes in retinal pigment epithelial detachments as a predictor for retreatment with anti-VEGF therapy. *Retina*. 2013;33:459–466.

44. Filho C, Penha FM, Gregori G, Rosenfeld PJ. Increasing volume of a retinal pigmented epithelial detachment as a predictor of submacular hemorrhage during anti-VEGF therapy. *Ophthalmic Surg Lasers Imaging Retina*. 2013;44: 204–207.

45. Lee KM. *Segmentations of the Intraretinal Surfaces, Optic Disc and Retinal Blood Vessels in 3D-OCT Scans* [doctoral thesis]. Iowa City, IA: University of Iowa; 2009.

46. Chen X, Niemeijer M, Zhang L, Lee K, Abramoff MD, Sonka M. Three-dimensional segmentation of fluid-associated abnormalities in retinal OCT: probability constrained graph-search-graph-cut. *IEEE Trans Med Imag*. 2012;31: 1521–1531.

47. Boykov Y, Veksler O, Zabih R. Fast approximate energy minimization via graph cuts. *IEEE Trans Pattern Anal Mach Intell*. 2001;23:1222–1239.

48. Haralick RM, Shanmugam K. Textural features for image classification. *IEEE Transactions Syst Man Cybern B Cybern*. 1973;610–621.

49. Fernandez DC. Delineating fluid-filled region boundaries in optical coherence tomography images of the retina. *IEEE Trans Med Imag*. 2005;24:929–945.

50. Goldstein T, Bresson X, Osher S. Geometric applications of the split Bregman method: segmentation and surface reconstruction. *J Sci Comp*. 2010;45:272–293.

51. Goldstein T, Osher S. The split Bregman method for L1-regularized problems. *SIAM J Imag Sci*. 2009;2:323–343.

translational vision science & technology

52. Pilch M, Stieger K, Wenner Y, et al. Automated segmentation of pathological cavities in optical coherence tomography scans. *Invest Ophthalmol Vis Sci.* 2013;54:4385–4393.

53. Cover T, Hart P. Nearest neighbor pattern classification. *IEEE Trans Inf Theory.* 1967;13: 21–27.

54. Hartigan JA. Statistical theory in clustering. *J Classification.* 1985;2:63–76.

55. LeCun Y, Bottou L, Bengio Y, Haffner P. Gradient-based learning applied to document recognition. *Proc IEEE.* 1998;86:2278–2324.

56. Quellec G, Lee K, Dolejsi M, Garvin MK, Abramoff MD, Sonka M. Three-dimensional analysis of retinal layer texture: identification of fluid-filled regions in SD-OCT of the macula. *IEEE Trans Med Imag.* 2010;29:1321–1330.

57. Niemeijer M, Lee K, Chen X, Zhang L, Sonka M, Abramoff MD. Automated estimation of fluid volume in 3D OCT scans of patients with CNV due to AMD. *Invest Ophthalmol Vis Sci.* 2012;53: 4074–4074.

58. Ding W, Young M, Bourgault S, et al. Automatic detection of subretinal fluid and sub-retinal pigment epithelium fluid in optical coherence tomography images. *Conf Proc IEEE Eng Med Biol Soc.* 2013;2013:7388–7391.

59. Garvin MK, Abramoff MD, Kardon R, Russell SR, Wu X, Sonka M. Intraretinal layer segmentation of macular optical coherence tomography images using optimal 3-D graph search. *IEEE Trans Med Imag.* 2008;27:1495–1505.

60. Breiman L. Random forests. *Machine Learning.* 2001;45:5–32.

61. Xu X, Lee K, Zhang L, Sonka M, Abramoff MD. Stratified sampling voxel classification for segmentation of intraretinal and subretinal fluid in longitudinal clinical OCT data. *IEEE Trans Med Imag.* 2015;34:1616–1623.

62. Vapnik V. *The Nature of Statistical Learning Theory.* New York: Springer; 1995.

63. Srinivasan PP, Kim LA, Mettu PS, et al. Fully automated detection of diabetic macular edema and dry age-related macular degeneration from optical coherence tomography images. *Biomed Opt Express.* 2014;5:3568–3577.

64. Liu YY, Ishikawa H, Chen M, et al. Computerized macular pathology diagnosis in spectral domain optical coherence tomography scans based on multiscale texture and shape features. *Invest Ophthalmol Vis Sci.* 2011;52:8316–8322.

65. Liu YY, Chen M, Ishikawa H, Wollstein G, Schuman JS, Rehg JM. Automated macular pathology diagnosis in retinal OCT images using multi-scale spatial pyramid with local binary patterns. *Med Image Anal.* 2011;15:748–759.

66. Liu YY, Chen M, Ishikawa H, Wollstein G, Schuman JS, Rehg JM. Automated macular pathology diagnosis in retinal OCT images using multi-scale spatial pyramid and local binary patterns in texture and shape encoding. *Med Image Anal.* 2011;15:748–759.

67. Serrano-Aguilar P, Abreu R, Anton-Canalis L, et al. Development and validation of a computer-aided diagnostic tool to screen for age-related macular degeneration by optical coherence tomography. *Br J Ophthalmol.* 2012;96: 503–507.

68. Viola P, Jones M. Rapid Object Detection Using a Boosted Cascade of Simple Features. Presented at: Proceedings of the 2001 IEEE international Conference on Symposium on Biomedical Imaging: Computer Vision and Pattern Recognition. December, 2001; Kauai, HI.

69. Quinlan J. *C4.5* Programs for Machine Learning. Burlington, MA: Morgan Kaufmann Publishers; 1993.

70. Lee SY, Stetson PF, Ruiz-Garcia H, Heussen FM, Sadda SR. Automated characterization of pigment epithelial detachment by optical coherence tomography. *Invest Ophthalmol Vis Sci.* 2012;53:164–170.

71. Albarrak A, Coenen F, Zheng Y. Age-related macular degeneration identification in volumetric optical coherence tomography using decomposition and local feature extraction. Presented at the 17th Annual Conference in Medical Image Understanding and Analysis (MIUA), July 2013, University of Birmingham, Birmingham, UK.

72. Zhang Y, Zhang B, Coenen F, Xiao J, Lu W. One-class kernel subspace ensemble for medical image classification. *EURASIP J Adv Signal Process.* 2014;2014:1–13.

73. Venhuizen FG, van Ginneken B, Bloemen B, et al. Automated age-related macular degeneration classification in OCT using unsupervised feature learning. *Proc SPIE.* 2015:94141I;94141I–94147I.

74. Kanagasingam Y, Bhuiyan A, Abramoff MD, Smith RT, Goldschmidt L, Wong TY. Progress on retinal image analysis for age related macular degeneration. *Prog Retin Eye Res.* 2014;38:20–42.

75. Wilkins GR, Houghton OM, Oldenburg AL. Automated segmentation of intraretinal cystoid fluid in optical coherence tomography. *IEEE Trans Biomed Eng.* 2012;59:1109–1114.

76. Lang A, Carass A, Swingle EK, et al. Automatic segmentation of microcystic macular edema in OCT. *Biomed Opt Express*. 2015;6:155–169.

77. Folgar FA, Chow JH, Farsiu S, et al. Spatial correlation between hyperpigmentary changes on color fundus photography and hyperreflective foci on SDOCT in intermediate AMD. *Invest Ophthalmol Vis Sci*. 2012;53:4626–4633.

78. Schuman SG, Koreishi AF, Farsiu S, Jung S-h, Izatt JA, Toth CA. Photoreceptor layer thinning over drusen in eyes with age-related macular degeneration imaged in vivo with spectral domain optical coherence tomography. *Ophthalmology*. 2009;116:488–496, e482.

79. Caselles V, Catté F, Coll T, Dibos F. A geometric model for active contours in image processing. *Numerische Mathematik*. 1993;66:1–31.

80. Xu C, Prince JL. Snakes, shapes, and gradient vector flow. *IEEE Trans Image Process*. 1998;7: 359–369.

translational vision science & technology